PAPER

Ultrasound standing wave spatial patterning of human umbilical vein endothelial cells for 3D micro-vascular networks formation

To cite this article: Huong Thi Le *et al* 2024 *Biofabrication* **16** 015009

Biofabrication

PAPER

Ultrasound standing wave spatial patterning of human umbilical vein endothelial cells for 3D micro-vascular networks formation

Huong Thi Le[1], Huu Lam Phan[1], Andreas Lenshof[2], Van Thuy Duong[1], Cholong Choi[3], Chaenyung Cha[3], Thomas Laurell[2,*] and Kyo-in Koo[1,4,*]

[1] Department of Electrical, Electronic and Computer Engineering, University of Ulsan, Ulsan 44610, Republic of Korea
[2] Department of Biomedical Engineering, Lund University, S-221 00 Lund, Sweden
[3] Department of Materials Science and Engineering, Ulsan National Institute of Science and Technology (UNIST), Ulsan, Republic of Korea
[4] Basic-Clinical Convergence Research Institute, University of Ulsan, Ulsan, Republic of Korea
[*] Authors to whom any correspondence should be addressed.

E-mail: thomas.laurell@bme.lth.se and kikoo@ulsan.ac.kr

RECEIVED
12 June 2023

REVISED
12 September 2023

ACCEPTED FOR PUBLICATION
16 October 2023

PUBLISHED
6 November 2023

Keywords: three-dimensional network structure, acoustofluidics, endothelial cell, tissue engineering

Supplementary material for this article is available online

Abstract

Generating functional and perfusable micro-vascular networks is an important goal for the fabrication of large and three-dimensional tissues. Up to now, the fabrication of micro-vascular networks is a complicated multitask involving several different factors such as time consuming, cells survival, micro-diameter vasculature and strict alignment. Here, we propose a technique combining multi-material extrusion and ultrasound standing wave forces to create a network structure of human umbilical vein endothelial cells within a mixture of calcium alginate and decellularized extracellular matrix. The functionality of the matured microvasculature networks was demonstrated through the enhancement of cell–cell adhesion, angiogenesis process, and perfusion tests with microparticles, FITC-dextran, and whole mouse blood. Moreover, animal experiments exhibited the implantability including that the pre-existing blood vessels of the host sprout towards the preformed vessels of the scaffold over time and the microvessels inside the implanted scaffold matured from empty tubular structures to functional blood-carrying microvessels in two weeks.

1. Introduction

The fabrication of full-size, sustainable, and functional three-dimensional (3D) organs is challenging because of the inability to create a dense microvascular network within the artificial organs [1]. The microvascular network is required for supplying nutrients and oxygen and performing metabolic by-products to sustain tissue metabolism and growth [2–4]. In addition, to avoid tissue necrosis and ischemic disorders, the maximum distance from a vessel to the farthest cell is limited to 100–200 μm [5, 6]. Therefore, rapid revascularization and generation of the functional vascular-dense network play important roles in the engineered tissue.

Endothelial cells (EC) are an important key to revascularization. Human umbilical vein endothelial cells (HUVEC) have been widely used as a source of primary EC for micro-vascularization because they represent the inner lining of blood vessels and play an important role in angiogenesis [7–9]. The vascular network can be formed via vasculogenesis, the *de novo* formation of blood vessels, or extended via angiogenesis, the growth of new vessels from pre-existing ones [10–14]. These processes could be optimized in an extracellular matrix (ECM) hydrogel, which can supply both physical and mechanical microenvironment for cells to survive and proliferate [15–18].

In the native structure, the microvascular networks are organized as a hierarchical distribution of progressive branching vessels, which is how blood is distributed throughout the tissues [19]. Hence, branching is a fundamental process that plays a critical role in the vessel network organization and functionality. For long-term survival and proper function of the engineered tissue, the vasculature networks

need to meet some requirements; (i) a 3D dense network to surpass the 200 μm diffusion limit of oxygen and nutrients, (ii) branching connections to cover the maximum tissue volume, (iii) functions of angiogenesis and perfusion, (iv) implantability to target host [20–24].

During the last few years, many research groups have been investigating pre-vascularized tissue constructs. Even though impressive results have been achieved, some limitations do remain. In bio-printing techniques the alignment of cell-laden layers are strictly required [12, 25] or only individual channels without any branching were made [26, 27]. A different approach is based on self-assembling abilities of ECs using drop-on demand technique [28]. ECs are encapsulated in droplets and printed onto a gel substrate. This approach does not facilitate generation of smaller vessels than the printed droplet and is time consuming to formulate the cell-spheroid.

As an alternative way, ultrasound-based approach is a well-known technique to manipulate the spatial location of cells. Ultrasound standing wave (USW) has been reported as a simple, fast, and non-invasive way for rapid patterning of microparticles and cells within 3D hydrogels [29–31]. Acoustic standing waves generates regions of pressure nodes and pressure anti-nodes and based on the cells size, density and compressibility, they can be acoustically moved toward the pressure nodes [32, 33]. Hence, this technique has the potential for various applications in bio-fabrication and biomaterial field such as vascular morphogenesis [31], myotubes organization [34], separation [35–37], and enrichment [38–40]. Previously, we have used an USW technique for aligning NIH/3T3 cells inside calcium alginate hydrogel. The combination of the continuous extrusion method and ultrasound cell manipulation resulted in cells arranged as branched structures. However, the aligned NIH/3T3 cells could not migrate well because animal cells could not degrade alginate [41].

In this study, we investigated the combination of a multi-material extrusion technique and USW to generate HUVECs in a network structure within a mixture of calcium alginate and decellularized extracellular matrix (dECM) from pig. Culturing the branching-structured scaffold with alginate lyase enabled the entrapped HUVECs to form a microvasculature network structure. Functionality and implantability of the matured microvasculature network were demonstrated.

2. Theory and concept

The method generated acoustic nodes inside the pre-hydrogel material to obtain a branched HUVEC structure and extruded three hydrogel layers for HUVECs' migration and maturing to vessels, as shown in figure 1. The USW at frequency 2 MHz in two types of square glass capillaries (400 μm and 800 μm) could generate transition from one focused cell stream to four cell streams of HUVECs and vice versa.

When applying 2 MHz ultrasound in a 400 μm square-shaped glass capillary, a half-wavelength standing wave was formed in both the x- and the y-direction with the pressure node in the channel center (figure 2(a)), which was described and demonstrated in our previous report [41]. When the capillary was doubled to 800 μm, the square capillary supported a full wavelength resonance in both the x- and y-directions and hence four pressure nodes were generated in the capillary cross-section, located $\lambda/4$ from the channel side walls (figure 2(b)).

Using red polystyrene microparticles, figure 3 demonstrates the principle of focusing particles or cells in in the acoustic standing wave field. The acoustic radiation force of the 2 MHz actuation in the 400 μm square capillary focused the microparticles into one stream at the center of the capillary (figure 3(b)). In the case of the 800 μm square capillary, four parallel lines of microparticles were generated in the sodium alginate. Due to their alignment at the regular quadrilateral points, some of the lines were obscured by the others when viewed under a two-dimensional microscope, as shown in figure 3(c). Based on this concept, alternating on and off 2 MHz ultrasound in the 400 μm and 800 μm square capillary patterned one line and four lines in a continuous linear structure, resulting in the branched and merged structure (figures 3(d)–(f)), and with HUVECs as shown in figure 1.

3. Results and discussion

3.1. Mixture of calcium alginate and dECM as a scaffold material

Via ionic crosslinking with calcium (Ca^{2+}) sodium alginate can form calcium alginate hydrogel rapidly [42, 43]. To preserve the branched cell structure inside the hydrogel, the pre-hydrogel material should be gellated as soon as possible right after the acoustic patterning. However, as shown in our earlier study [41] the animal cells could not migrate and proliferate well in calcium alginate because it cannot synthesize endogenous alginase for alginate degradation [44].

Therefore, a mixture of dECM from pig (figure S1) and sodium alginate at 9:1 of ratio was utilized as pre-hydrogel in this study. The dECM hydrogel has both characteristics of holding cells as scaffolds and working as functional ECM. It contains functional components of native tissue including collagen fibers, glycosaminoglycans, growth factors, and more. Therefore, it provides an excellent extracellular

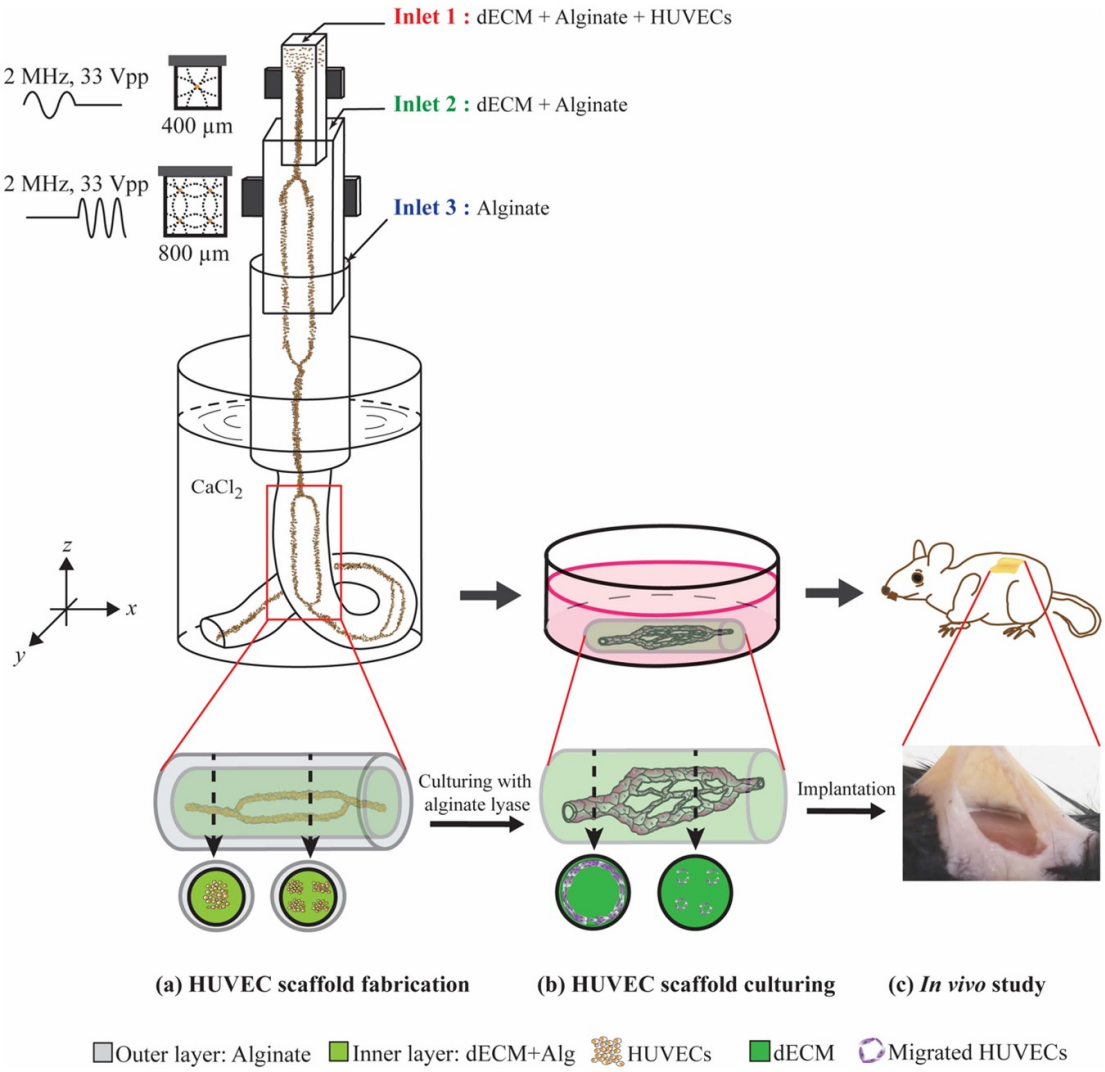

Figure 1. Schematic of the HUVECs patterning in hydrogel using ultrasound and the following in vivo study. (a) The HUVEC scaffold fabrication using the ultrasound standing waves. (b) The HUVEC scaffold culturing with alginate lyase. (c) The implantation of the matured HUVEC scaffold.

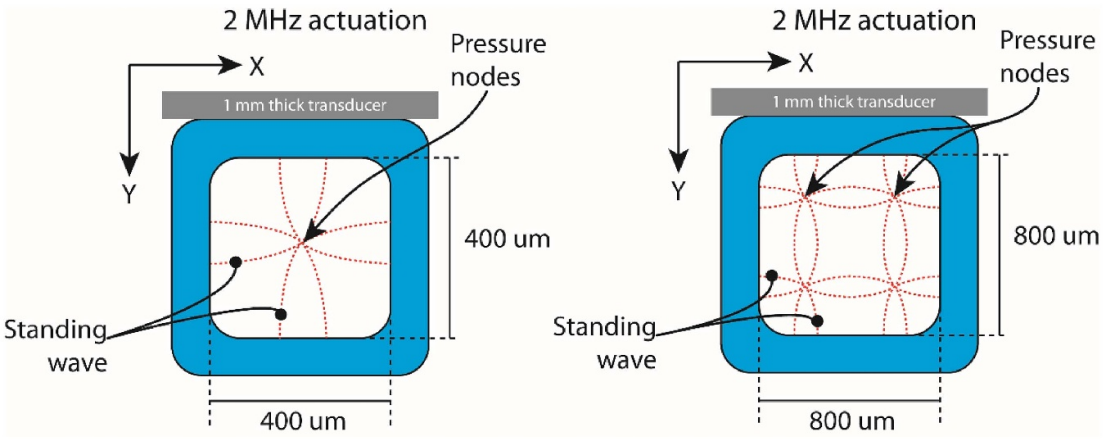

Figure 2. Schematic of the standing wave pattern in the capillary cross-section when actuated (a) at 2 MHz in 400 μm square-shaped glass capillary, yielding a single pressure node in the center for microparticle or cell focusing, and (b) at 2 MHz in the 800 μm square-shaped glass capillary, providing four pressure nodes, one in each cross-section quadrant for microparticle or cell focusing. The transducer dimensions are not to scale in the drawing.

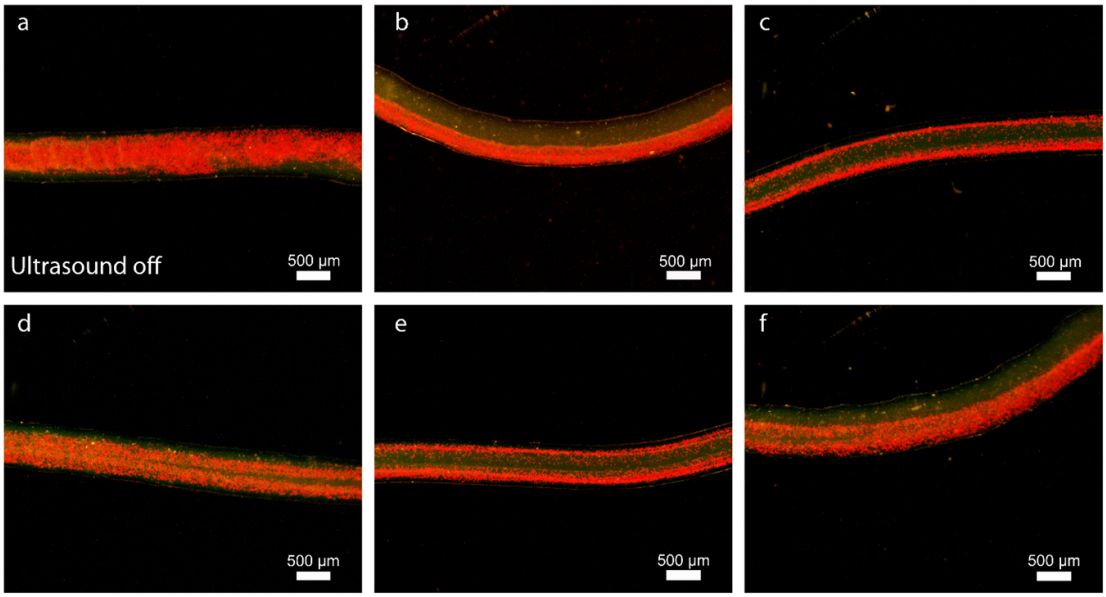

Figure 3. The polystyrene microparticle (red) in the mixture of the sodium alginate and the dECM. (a) The microparticles unexposed to ultrasound. (b) The aligned microparticles as one stream by the ultrasound. (c) The aligned microparticles as four streams by the ultrasound. (d) The patterned microparticles in transition from one stream to four streams. (e) The aligned microparticles as four streams. (f) The patterned microparticles in transition from four streams to one stream. The top view obscures the two underlying particle lines.

microenvironment for cells adhesion, differentiation, proliferation, and functional expression [45–47].

Figures 4(a)–(d) showed the microstructure of dECM, calcium alginate, mixture of calcium alginate and dECM, and the mixture of the calcium alginate and the dECM treated with alginate lyase, respectively. The dECM and the lyase-treated dECM presented more fibrous structure and higher porosity compared to calcium alginate only. These characteristics provided better microenvironment for cell adhesion and migration. In the mixture of dECM and calcium alginate, fiber diameter and pore size increased. This change might be due to the cross-liking reaction between $CaCl_2$ and dECM molecules [48].

The experimental outcomes further reveal that calcium alginate scaffold exhibits the most favorable mechanical properties, marked by the highest breaking force results, but the lowest diffusibility. On the other hand, the dECM scaffold shows the best diffusibility, it presents challenges in terms of handling. Meanwhile, the scaffold with mixture of calcium alginate and dECM can be easy to handle while maintaining adequate diffusibility. The lyase-treated dECM without cell showed low mechanical property but the cell-laden one has enough durability for implantation handling (figures 4(e), (g) and supplementary video 1).

3.2. Branched structure with HUVECs

For 3D vascular network formation, HUVECs were patterned alternating in a single line and in four lines. From the cross-section image (figures 5(a) and (b)), four groups of manipulated cells were distinguishable corresponding to the acoustic nodal positions. The extraction of beam intensity from cross-sectional confocal images also showed that particles were concentrated at specific locations corresponding to the acoustic nodes (figure 5(c)).

It is well known that cell concentration and acoustic power significantly influenced the patterned structures [31, 49, 50]. In our hydrogel mixture, 1×10^6, 5×10^6 and 8×10^6 cells ml^{-1} of HUVECs were patterned using an actuation voltage of 20 V_{PP} and 33 V_{PP}, as shown in figure S2. As the cell concentration and the acoustic power increased, the width of the grouped cells and inter-distance between the groups also increased.

Temperature measurement on the backside of the transducers after ten-minute operating at 33 V_{PP} saturated under 40 °C (figure S3), which is the upper limit temperature condition of the hydrogel for the cell viability [51]. Live and dead cell fluorescent images of the 33 V_{PP} scaffold was not easy to discriminate from those of the 20 V_{PP} scaffold (figure S4). Cell viabilities of scaffolds made at both actuation voltages was found to be about 90% (figure S5)

3.3. Enhanced HUVEC proliferation by alginate enzyme

It is known that animal cells have no receptors to recognize alginate which is required for signaling production between cells and external matrix interaction [52, 53]. This results in limited animal cell proliferation in an alginate scaffold. Therefore,

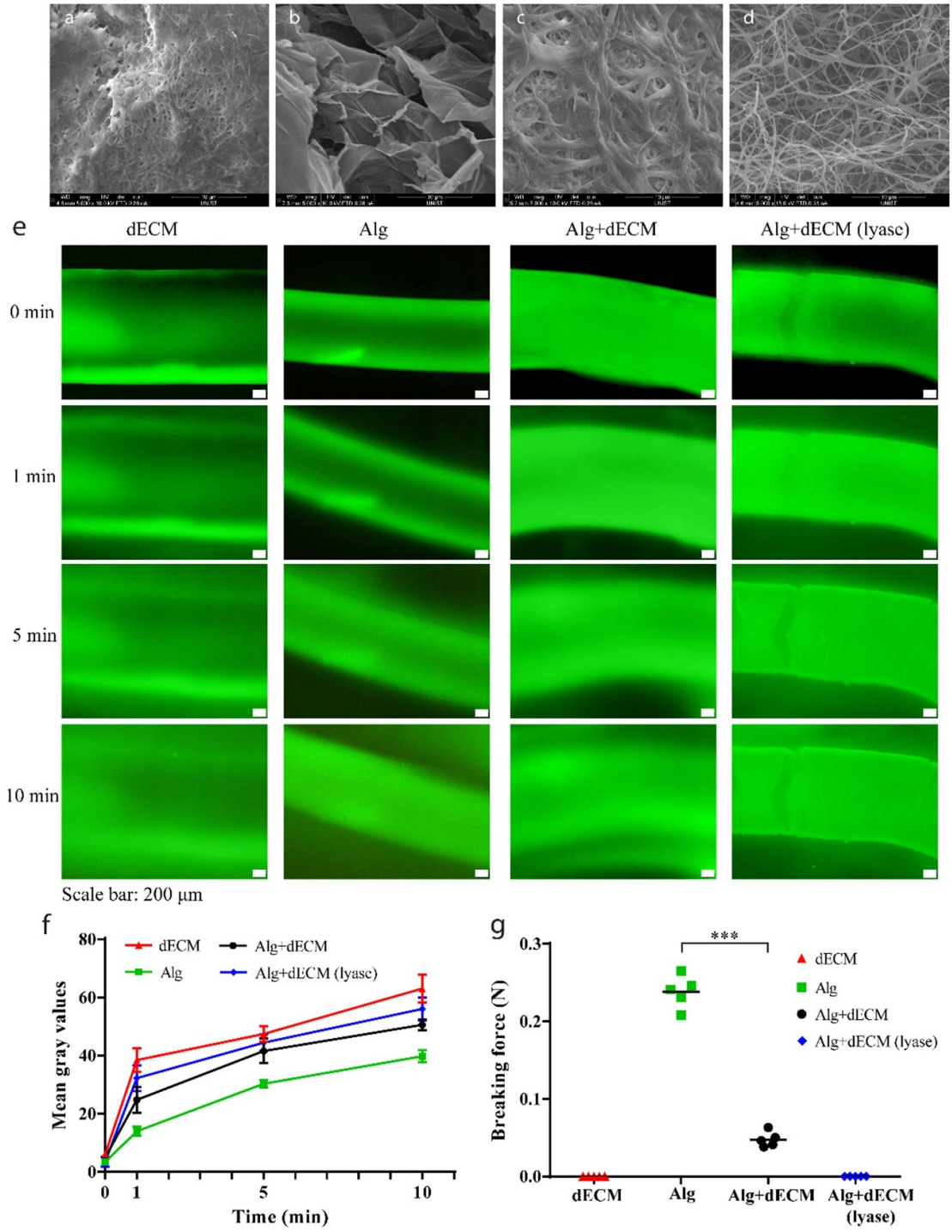

Figure 4. Scanning electron microscopy (SEM) images of (a) the dECM hydrogel, (b) the calcium alginate hydrogel, and (c) the mixture of the calcium alginate and the dECM. (d) the mixture of the calcium alginate and the dECM treated with alginate lyase. (e) Time-lapse fluorescent images of FITC-Dextran diffusion of the dECM, the calcium alginate, and the mixture of the calcium alginate, and the mixture of the calcium alginate and the dECM treated with alginate lyase hydrogel scaffold from 0 min to 10 min. (f) The fluorescent intensity was analyzed with respect to the time (n = 3). (g) The breaking force of the hydrogel scaffold (*** $p < 0.001$, n = 5).

in this manuscript, HUVECs scaffolds were cultured together with alginate lyase which degrades alginate through breaking glycosidic bond [54]. The microstructure of the mixture of dECM and calcium alginate scaffold after the degradation of calcium alginate showed the fibrous structure which can serve as a supportive ECM for cell growth (figure 4(d)).

The HUVEC scaffold cultured with alginate lyase exhibited more cell–cell adhesion and better lumen formation than the non-lyase scaffold in the one-line

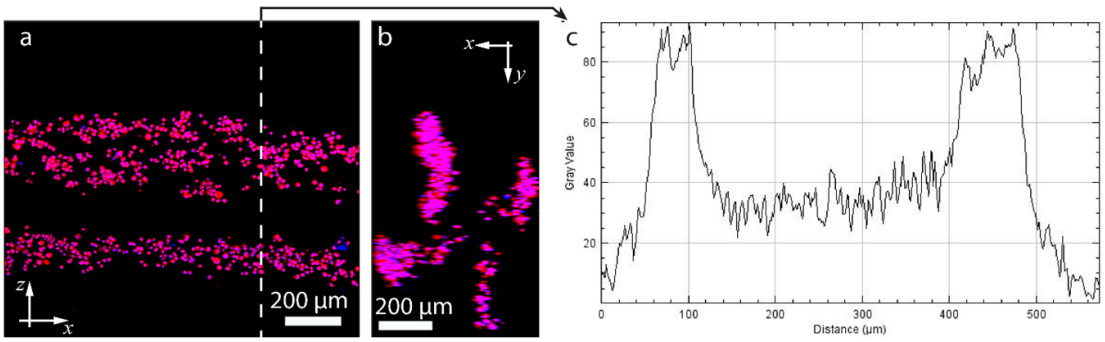

Figure 5. Confocal microscope image of the aligned RFP-HUVECs aligned as four lines. (a) The longitudinal view and (b) the z-stack image reconstructed cross-sectional views. (c) Spatial distribution of the fluorescence intensity in (a).

region (figures 6(e) and (f)). In the four-line region, the HUVEC scaffold with lyase appear to show a more lumen like formation than the non-lyase scaffold. (figures 6(g) and (h)). This trend is presented in the cell-occupying ratio graph and the cell perimeter graph (figures 6(i), (j) and S6) as well. The cell-occupancy of the lyase-culturing scaffold increased from 60.4 ± 6.8% at day 1–91.6 ± 4.7% at day 7, as compared to the non-lyase scaffold, 24.9 ± 4.9% at day 1 to % 45.8 ± 4.2% at day 7. In case of the cell perimeter, the difference with and without the lyase was about two times at day 7.

3.4. Microvascular network formation

EC constitute the inner side of all vessel types as a monolayer, named as endothelium [55–58]. Adjacent EC link each other through inter-endothelial junctions, which are categorized as adherens junctions, tight junctions and gap junctions. These junctions play an essential role in tissue integrity, barrier function and cell–cell communication, respectively. The HUVEC scaffold cultured with alginate lyase expressed CD31 (a biomarker of platelet endothelial cell adhesion), ZO-1 (a biomarker of the tight junction), and VE-cadherin (a biomarker of the adherens junction) as shown in figures 7(a)–(c), respectively. The presence of these markers indicated the junctions among adjacent cells and the maturity of EC to form the vascular network [50, 59].

The lyase-culturing HUVEC scaffold with high cell density (8×10^6 cells ml^{-1}) showed much more angiogenic sprouting in the one-line region and more cell–cell network formation in the four-line region than the non-lyase scaffold (figure 8). Angiogenic sprouting number in the lyase culturing increased from about 10.4 ± 1.7 at day 3–16.2 ± 1.9 at day 9. Its sprout length increased from 80.8 ± 11.1 μm at day 3–191.0 ± 25.8 μm at day 9 as well. Furthermore, the distance between vessels were almost less than 100 μm (figure S7) The formation of the dense microvascular networks demonstrates a potential for volumetric artificial tissue to overcome the maximum diffusion distance from microvessels, 200 μm [60, 61]. In contrast, in the lyase-less HUVEC scaffold cells were disconnected and presented no angiogenic sprouting. In case of the cell density is lower (1×10^6 cells ml^{-1}), the cells create sparse networks and do not exhibit any angiogenic sprouting (figure S8).

Until day 3, the cell area coverage and cell perimeter have increased dramatically (figures 6(i) and (j)). Since day 3, the sprout number and length have increased gradually (figures 8(g) and (h)). Especially, the sprout length increased abruptly from day 5 to day 9. This observation was similar with the previous reports [23, 62]

3.5. Perfusability

Perfusion is one of the crucial properties in vasculature to induce a stable circulatory system or lymphatic system to an organ or tissue [63, 64]. To evaluate the perfusability of the fabricated microvascular networks different fluids, such as food dye, fluorescent microparticles, FITC-dextran, and whole mouse blood were pumped into the lyase-cultured HUVEC scaffold using a lab-made connector (figure S9(a)). As shown in figures S9(b) and (c), food dye could successfully be perfused inside the HUVEC scaffold. After perfusing with red 5 μm microparticles some of the microparticles, figure S10(b), could be found adhering to the inside of the one-line region. Likewise, FITC-dextran 70 kDa was perfused through the fabricated vasculature network and out of the HUVEC scaffold without leakage (Supplementary Video 2). In the four-line region, some FITC-Dextran (the green one in figures S11(b)–(d)) were found after pumping. After pumping whole mouse blood, some red blood cells (the pink arrows in figure 9(c)), analogous to the microparticle perfusion, were found on the inside of the lumen in the network region. The perfusion experiments demonstrates that the achieved vasculature network demonstrated an intact

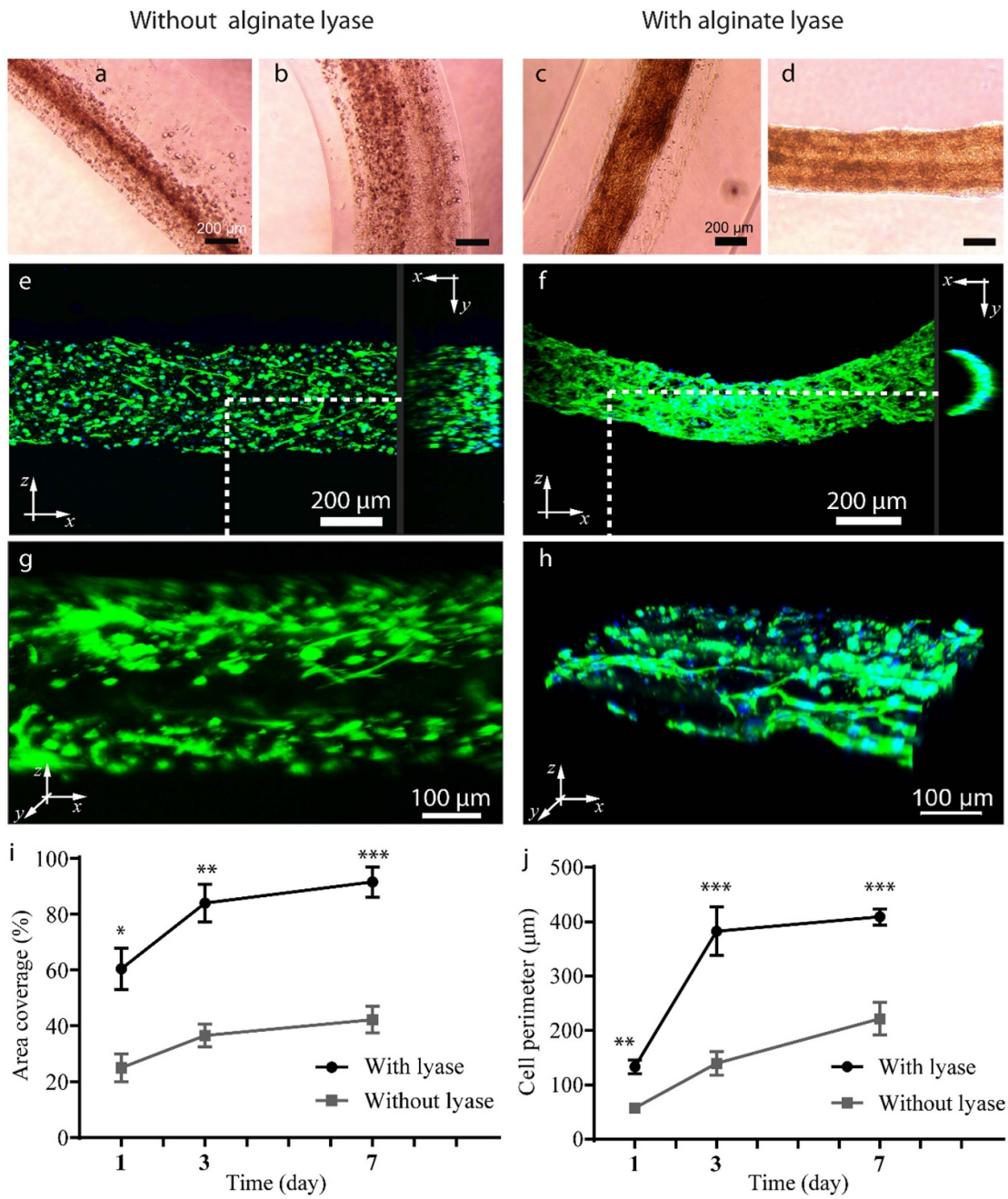

Figure 6. The HUVECs scaffold culturing without and with the alginate degradation. The bright-field images (a), (b) without and (c), (d) with the alginate degradation. (e) No hollow formation in one line region in case of no alginate degradation at day 3. (f) The hollow channel in one line region after 3 d culturing with the alginate degradation. The four lines region (g) without the alginate degradation and (h) with the alginate degradation (green: F-actin, blue: DAPI). (i) The area coverage according to the culturing time in both cases (* $p < 0.05$, ** $p < 0.01$, *** $p < 0.001$ comparing between with lyase and without lyase, $n = 3$). (j) The cell perimeter according to the culturing time in both cases, (** $p < 0.01$, *** $p < 0.001$ comparing between with lyase and without lyase, $n = 100$).

endothelium considering the expressed biomarkers and its ability to confine the perfused fluids inside the lumen.

3.6. Subcutaneous implantation

To estimate implantablity of the HUVEC network scaffold, it was grafted under the mouse dorsal skin as shown in figures S12(a)–(e). After surgery, the transplanted region recovered quickly with neither swelling nor inflammation. The operated skin was mostly recovered after 7 d, and hair regrew after 14 d. Under bright field microscopy, blood vessels in the extracted tissue were observed as well (figures S12 (f)–(h)).

Histological analysis with hematoxylin and eosin (H&E) staining (figure 10) and Masson's trichrome

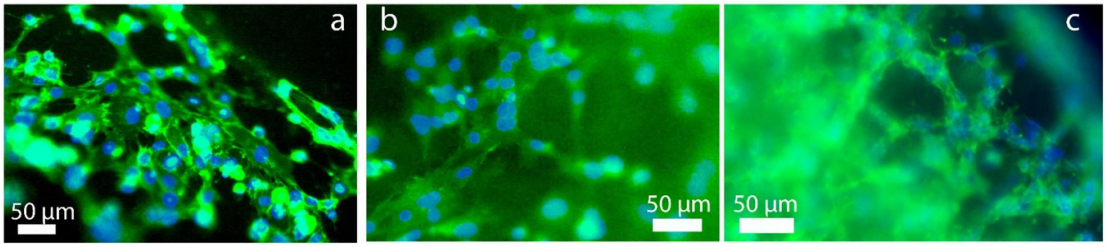

Figure 7. The immunofluorescent staining with (a) CD31 (green) (a) biomarker of platelet endothelial cell adhesion, (b) ZO-1 (green) (a) biomarker of the tight junction, and (c) VE-cadherin (green) (a) biomarker of the adherens junction, in the HUVECs scaffold after 3 d culturing with the alginate lyase. The blue is DAPI.

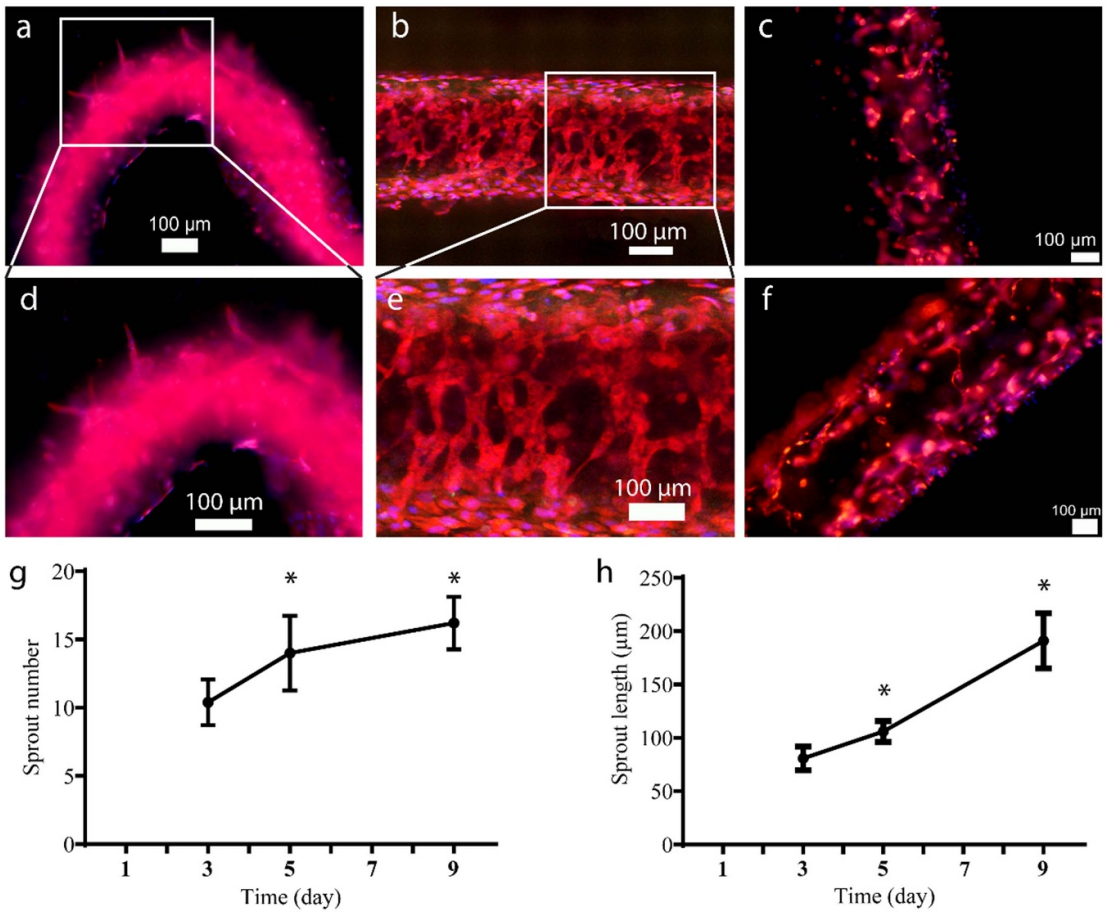

Figure 8. The fluorescent images of the RFP-HUVEC (a) and (d) in the one-line region and (b) and (e) in the four-line region after 3 d of culturing with the alginate lyase. (c) and (f) The fluorescent images of the RFP-HUVEC after 3 d culturing without any alginate lyase in the one-line and four-line region, respectively. The red is RFP-HUVEC. (g) The sprout number and (h) the sprout length according to the culturing time with the alginate lyase (* $p < 0.05$, compared with day 3, $n = 5$).

staining (figure 11) further showed efficient incorporation of the implanted scaffold into the host tissue. As time went from the implanting surgery, red blood cells were observed in smaller lumens (figures 10(d)–(f)). At day 3, the smallest lumen having red blood cell is 12.1 μm in diameter. The smallest lumen decreased as 8.1 μm at day 14. These findings supposed that the plural microvessels inside the implanted scaffold evolved from empty tubular structures to functional blood-carrying microvessels and the implanted scaffold formulated with human EC anastomosed with the existing vasculature of the host. Furthermore, Masson's trichrome staining showed that the collagen fibers—as the representative of the ECM surrounding the cells site—considerably increased within the grafted tissue after 14 d implantation (figure 11). These results were an indicator of a good incorporation with the host tissue.

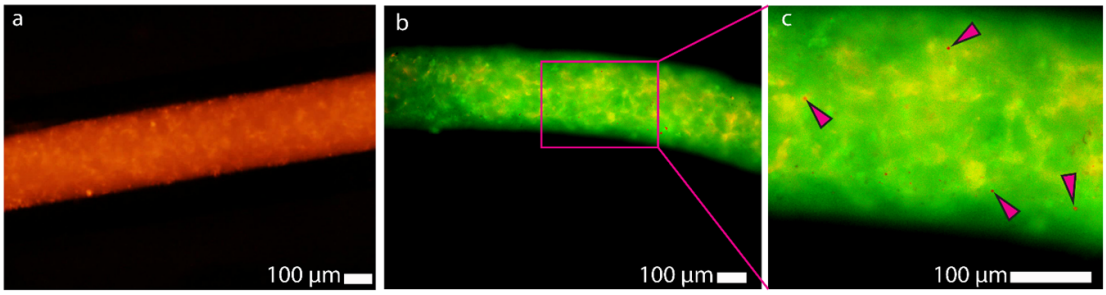

Figure 9. The perfusability test of the HUVECs microvascular network with mouse blood. (a) The fluorescent images of the RFP-HUVEC microvascular network scaffold (light red) before pumping. (b), (c) the fluorescent images in the network region after pumping mouse blood. The pink arrows point the red blood cells of the mouse blood. The dark red is a red blood cell. The green is cell tracker dye.

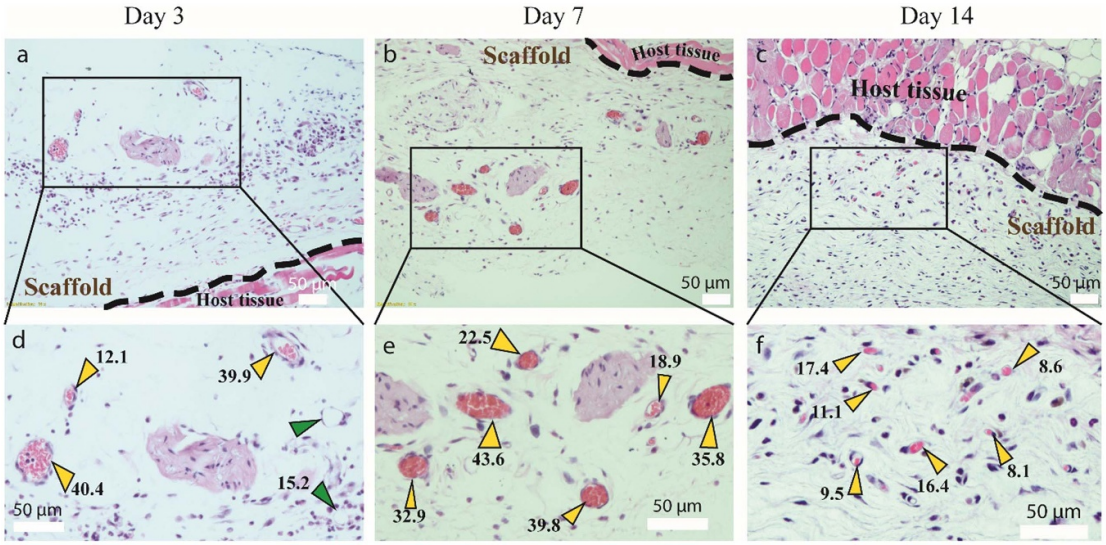

Figure 10. The hematoxylin and eosin (HE) staining images of the scaffold implanted in the mouse dorsal for (a), (d) 3 d, (b), (e) 7 d, and (c), (f) 14 d, respectively. The yellow arrow points microvessel carrying red blood cells. The numbers are diameters of the lumens. The green arrow indicates the empty lumens. The pink is an ECM. The purple is nuclei. The bright red is red blood cell.

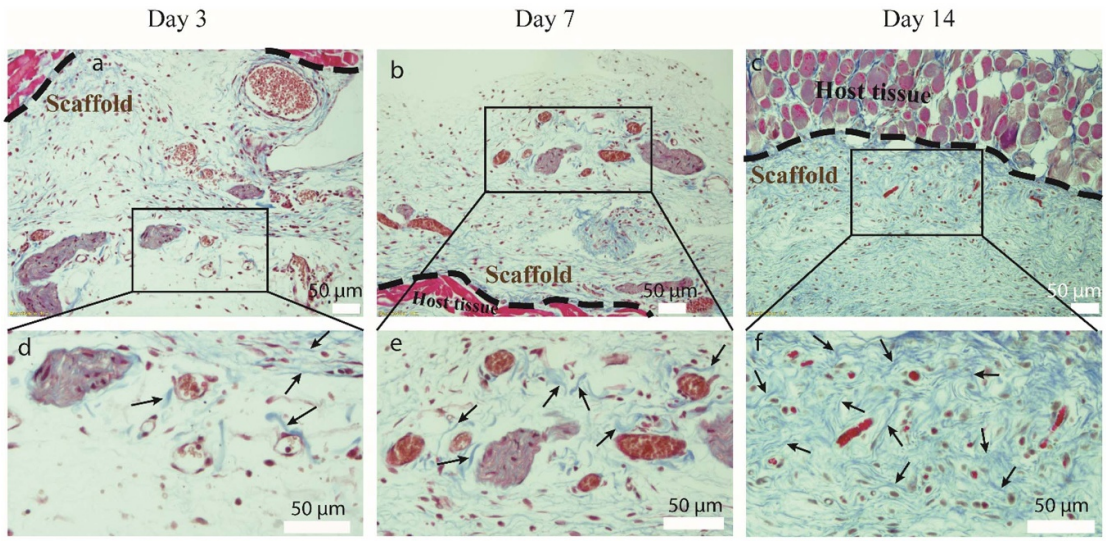

Figure 11. The Masson's trichrome staining images of the scaffold implanted in the mouse dorsal for (a), (d) 3 d, (b), (e) 7 d, and (c), (f) 14 d, respectively. The microvessels can be recognized as lumen structures carrying red blood cells. The pink is cytoplasm. The black is nuclei. The blue is collagen fibers and ECM. The black arrowhead points to collagen fibers. The red is red blood cell.

4. Conclusion

We developed a vasculature network using the combination of acoustic standing wave forces and multi-hydrogel extrusion. The patterned EC matured as functional vessel network such as angiogenesis, perfusability, and implantability. If the developed approach integrates with target organ cells such as liver cells, it could potentially pave the route to generate fully vascularized artificial organ. Due to the fully networked vasculatures, the artificial organ would be implant-ready even after a relatively short *in vitro* maturing time. Currently we are investigating an artificial liver construct using the developed approach in this study.

5. Materials and methods

5.1. Hydrogel preparation

Three hundred fifty milligram dECM powder and 200 mg pepsin (Sigma-Aldrich, St. Louis, MO, U.S.A.) dissolved in 1 ml acetic acid (Sigma-Aldrich, St. Louis, MO, U.S.A.) and DI water to make 35 mg ml^{-1} concentration dECM of 100 ml total volume solution. The solution was stirred for 72–96 h at room temperature (RT). After that, the dissolved dECM was centrifuged at 3000 rpm for 15 min. The supernatant was carefully transferred into other conical tubes, and then the remained non-dissolved components were discarded. The tubes containing dissolved dECM was kept in storage at 2 °C–8 °C.

For dECM neutralization and dilution, the 35 mg ml^{-1} dECM was mixed with 10 M and 1 M NaOH (Sigma-Aldrich, St. Louis, MO, U.S.A.) and 10X PBS (10% of the total volume) to adjust pH range from 7.2 to 7.5 and 25 mg ml^{-1} dECM concentration (figure S1). Final hydrogel for acoustic pattering was a mixture of sodium alginate (MERCK, Madison, NJ, U.S.A.) (0.5% w/v) and dECM (25 mg ml^{-1}) at ratio 1:9. All these steps were processed on ice to avoid gellation.

5.2. Cell culture

HUVEC were purchased from ATCC (PCS-100–010, cryopreserved, ATCC, U.S.A.). Cell culture medium included EGMt-2 Endothelial Cell Growth Medium-2 Bullet Kit (Lonza, Basel, Switzerland) and 1% penicillin/streptomycin (Sigma-Aldrich, St. Louis, MO, U.S.A.). The HUVECs were seeded on cell culture polystyrene dishes and incubated at 37 °C and 5% CO_2. The cells within passages 6–10 were used in experiments.

5.3. Multi-line patterning using ultrasound

As shown in figures 1, 1 mm thick ultrasound transducers (MEGITT A/S, Kvistgaard, Denmark) glued to a 400 μm and an 800 μm square-shaped glass capillaries (VitroCom, NJ, U.S.A.) respectively. The device has three inlets. The mixture of sodium alginate and dECM was mixed with 60 μl of 10 micrometer (diameter) polystyrene microparticles (MERCK, Madison, NJ, U.S.A.) and was pumped into the inlet 1. The same ratio of dECM and alginate without any microparticles was supplied into the inlet 2. Sodium alginate (1% w/v) was injected into the inlet 3. The flow rate for the inlet 1 is 30 μl min^{-1}, the inlet 2 is 30 μl min^{-1} and the inlet 3 is 150 μl min^{-1}. For cell experiments, 100 μl of HUVECs was used instead of the microparticles. The outlet was immersed into a beaker of 300 mM $CaCl_2$ (MERCK, Madison, NJ, U.S.A.) for cross-linking.

5.4. Microvascular network formation

The extruded cell-laden scaffolds were cultured in conventional HUVEC media described previously for one day at 37 °C and 5% CO_2 to maintain the extruded three-layered structures intact. After one day of the conventional culturing, alginate lyase enzyme (MERCK, Madison, NJ, U.S.A.) was added into the conventional HUVEC media at a final concentration of 0.1 unit/mL to dissolve calcium alginate ingredients in the layered scaffolds for HUVEC migration. The alginate-degrading media was replaced every day.

5.5. Mice

The C57BL/6 mice (3–8 weeks old, 15–35 g) were purchased from KOATECH (Pyeongtaek, Republic of Korea). The mice were kept in a facility with 60% humidity at 24 °C, a 12 h light/dark cycle, and free access to drinks and food. Animal studies were performed in line with the principles and guidelines of laboratory animal care and ethics, with permission from the University of Ulsan's Institutional Animal Care and Use Committee (GIG-22–030 and GIG-22–040, University of Ulsan, Ulsan, Republic of Korea). The experiment was conducted three times using a total of nine mice.

5.6. Whole blood collection and labelling (cell tracker)

Mouse whole blood was collected using tail vein collection technique [65]. One milliliter of whole blood was collected from a 20–30 g mouse. The gathered whole blood was mixed with heparin (Sigma, U.S.A.) at 30 USP units/mL as the final concentration. The heparinated whole blood was incubated with a cytoplasmic probe and 10 μM Cell Tracker™ Green BODIPY™ dyes (C2102, Thermo Scientific, U.S.A.) for 35 min following manufacturer's instructions before perfusing.

5.7. Perfusablility assay

A lab-made connector (supplement figure 7(a)) holds the matured scaffold using additional calcium alginate hydrogel. To secure pumping, a glass capillary (ID: 50 μm, OD: 80 μm, VitroCom, NJ, U.S.A.), the red one in supplement figure 7(a), was inserted into a vessel of the matured scaffold. Solutions such as 5 μm fluorescent microparticles, whole blood of mouse, or fluorescein isothiocyanate dextran (FITC-dextran) 70 kDa was injected at a constant flow of 15 μl min^{-1}. After perfusing for 5 min, the HUVEC scaffold was washed with 1X PBS buffer for microscope observation.

5.8. Implant surgery

A mouse (6–8 weeks and 20–30 g) was anesthetized using 2,2,2-Tribromoethanol ($\sim$240 mg kg^{-1}) (Sigma-Aldrich, St. Louis, MO, U.S.A.). The hair was removed by Nair gel (Church& Dwight UK Ltd, Kent, U.K.) and povidone-iodine 10% (Forson, Chungcheongnam, Republic ok Korea) applied for disinfection before surgery. The skin on the back of the mouse opened about $\sim$ 30 mm in length and $\sim$ 20 mm in wide using scissors and fine forceps. The matured scaffold ($\sim$ 2 cm in length) was placed under the skin. After that, the open skin was closed using black silk suture 4–0 (Ailee, BU.S.A.n, Republic of Korea). The implanted mouse was kept in warm for 3–4 h to recover. The mouse was recovered separately and its inflammation after the surgery was monitored visually during the recovery time. For harvesting the implanted scaffold, the operated mouse was anesthetized one more time on day 3, 7 and 14. After harvesting, the anesthetized mouse was performed cervical dislocation until respiration has stopped for euthanasia. All surgical instruments were autoclaved before the experiments.

5.9. Immunofluorescent staining

The HUVECs scaffold were fixed in 4% paraformaldehyde (Sigma-Aldrich, St. Louis, MO, U.S.A.) for 25 min at RT, permeabilized with 0.5% Triton-X100 (Sigma-Aldrich, St. Louis, MO, U.S.A.) for 5 mininutes, and then treated with 5% bovine serum albumin (BSA) (Sigma-Aldrich, St. Louis, MO, U.S.A.) as blocking solution for 20 min at RT. The primary antibody CD31 (1:50) (Thermo Scientific, Waltham, Massachusetts, U.S.A.), ZO-1 (1:100) (Thermo Scientific, Waltham, Massachusetts, U.S.A.), VE-cadherin (1:100) was incubated with the treated scaffolds at 4 °C overnight. Subsequently, the scaffolds were incubated with a goat anti-mouse IgG (H + L) highly cross adsorbed secondary antibody, Alexa Fluor plus 488 (1:1000) (Thermo Scientific, Waltham, Massachusetts, U.S.A.) for 120 min at RT. The nuclei were stained with 4′,6-diamidino2-phenylindole (DAPI) (NucBlue® Live ReadyProbes™ Reagent, Thermo Scientific, Waltham, Massachusetts, U.S.A.) for 15 min before imaging. The scaffolds were washed with 1X PBS buffer (3 time/5 min) between steps.

5.10. Imaging and statistical analyses

The cell-stained scaffolds were observed with an IX53 inverted fluorescent microscope (Olympus, Tokyo, Japan), and pictures were taken with CellSens software (Olympus, Tokyo, Japan). A laser scanning confocal microscope (FLUOVIEW FV1200, Olympus, Tokyo, Japan) was used for 3D imaging. All data were shown as the mean $\pm$ standard deviation (SD). ImageJ (NIH, Washington, U.S.A.) was used for image preparation and analysis.

Data availability statement

The data cannot be made publicly available upon publication because no suitable repository exists for hosting data in this field of study. The data that support the findings of this study are available upon reasonable request from the authors.

Acknowledgments

Huong Thi Le, Huu Lam Phan, Van Thuy Duong, and Kyo-in Koo were supported by Korean Medical Device Development Fund (RS2021-KD000013), Republic of Korea. Thomas Laurell and Andreas Lenshof were supported by the Swedish Research Council, Grant Number 2019-00795.

Author contributions

Conceptualization, H T L and K-i K; methodology, K-i K, H T L, A L and H L P; conducted experiment H T L V TD, C Cha and C Choi; project administration, K-i K and T L; writing—original draft, H T L and K-i K; writing—review and editing, A L and T L. All authors have read and agreed to the published version of the manuscript.

Conflict of interest

The authors declare no competing interests.

ORCID iDs

Huong Thi Le https://orcid.org/0000-0001-6657-4523
Huu Lam Phan https://orcid.org/0000-0002-2025-5946
Andreas Lenshof https://orcid.org/0000-0003-2887-6365
Van Thuy Duong https://orcid.org/0000-0002-7131-4272
Cholong Choi https://orcid.org/0000-0001-9722-8842

Chaenyung Cha https://orcid.org/0000-0002-3615-0145
Thomas Laurell https://orcid.org/0000-0002-2486-3607
Kyo-in Koo https://orcid.org/0000-0003-4173-9218

References

[1] Kang B, Shin J, Park H-J, Rhyou C, Kang D, Lee S-J, Yoon Y-S, Cho S-W and Lee H 2018 High-resolution acoustophoretic 3D cell patterning to construct functional collateral cylindroids for ischemia therapy *Nat. Commun.* **9** 5402
[2] Cui H *et al* 2019 In vitro and in vivo evaluation of 3D bioprinted small-diameter vasculature with smooth muscle and endothelium *Biofabrication* **12** 015004
[3] Rouwkema J and Khademhosseini A 2016 Vascularization and angiogenesis in tissue engineering: beyond creating static networks *Trends Biotechnol.* **34** 733–45
[4] Tiruvannamalai Annamalai R, Rioja A Y, Putnam A J and Stegemann J P 2016 Vascular network formation by human microvascular endothelial cells in modular fibrin microtissues *ACS Biomater. Sci. Eng.* **2** 1914–25
[5] Asakawa N, Shimizu T, Tsuda Y, Sekiya S, Sasagawa T, Yamato M, Fukai F and Okano T 2010 Pre-vascularization of in vitro three-dimensional tissues created by cell sheet engineering *Biomaterials* **31** 3903–9
[6] Grainger S J and Putnam A J 2011 Assessing the permeability of engineered capillary networks in a 3D culture *PLoS One* **6** e22086
[7] Hauser S, Jung F and Pietzsch J 2017 Human endothelial cell models in biomaterial research *Trends Biotechnol.* **35** 265–77
[8] Davis J, Crampton S P and Hughes C C W 2007 Isolation of human umbilical vein endothelial cells (HUVEC) *J. Vis. Exp.* **3** e183
[9] Kocherova I *et al* 2019 Human umbilical vein endothelial cells (HUVECs) co-culture with osteogenic cells: from molecular communication to engineering prevascularised bone grafts *J. Clin. Med.* **8** 1602
[10] Song J, Miermont A, Lim C T and Kamm R D 2018 A 3D microvascular network model to study the impact of hypoxia on the extravasation potential of breast cell lines *Sci. Rep.* **8** 17949
[11] Park Y K, Tu T-Y, Lim S H, Clement I J M, Yang S Y and Kamm R D 2014 In vitro microvessel growth and remodeling within a three-dimensional microfluidic environment *Cell Mol. Bioeng.* **7** 15–25
[12] Park J Y, Ryu H, Lee B, Ha D-H, Ahn M, Kim S, Kim J Y, Jeon N L and Cho D-W 2018 Development of a functional airway-on-a-chip by 3D cell printing *Biofabrication* **11** 015002
[13] Vailhé B, Vittet D and Feige J-J 2001 In vitro models of vasculogenesis and angiogenesis *Lab. Invest.* **81** 439–52
[14] Lesman A, Rosenfeld D, Landau S and Levenberg S 2016 Mechanical regulation of vascular network formation in engineered matrices *Adv. Drug Deliv. Rev.* **96** 176–82
[15] Porzionato A, Sfriso M M, Macchi V, Rambaldo A, Lago G, Lancerotto L, Vindigni V and De Caro R 2013 Decellularized omentum as novel biologic scaffold for reconstructive surgery and regenerative medicine *Eur. J. Histochem.* **57** e4
[16] Giobbe G G *et al* 2019 Extracellular matrix hydrogel derived from decellularized tissues enables endodermal organoid culture *Nat. Commun.* **10** 5658
[17] Aamodt J M and Grainger D W 2016 Extracellular matrix-based biomaterial scaffolds and the host response *Biomaterials* **86** 68–82
[18] Duong V T, Nguyen C T, Phan H L, Le V P, Dang T T, Choi C, Seo J, Cha C, Back S H and Koo K-I 2023 Double-layered blood vessels over 3 mm in diameter extruded by the inverse-gravity technique *Biofabrication* **15** 045022
[19] Pries A R and Secomb T W 2014 Making microvascular networks work: angiogenesis, remodeling, and pruning *Physiology* **29** 446–55
[20] Santos M I and Reis R L 2010 Vascularization in bone tissue engineering: physiology, current strategies, major hurdles and future challenges *Macromol. Biosci.* **10** 12–27
[21] Laschke M W, Mussawy H, Schuler S, Kazakov A, Rücker M, Eglin D, Alini M and Menger M D 2010 Short-term cultivation of in situ prevascularized tissue constructs accelerates inosculation of their preformed microvascular networks after implantation into the host tissue *Tissue Eng.* A **17** 841–53
[22] Pill K, Melke J, Mühleder S, Pultar M, Rohringer S, Priglinger E, Redl H R, Hofmann S and Holnthoner W 2018 Microvascular networks from endothelial cells and mesenchymal stromal cells from adipose tissue and bone marrow: a comparison *Front. Bioeng. Biotechnol.* **6** 156
[23] Nguyen C T, Duong V T, Hwang C H and Koo K I 2022 Angiogenesis in free-standing two-vasculature-embedded scaffold extruded by two-core laminar flow device *Int. J. Bioprint.* **8** 557
[24] Duong V T, Dang T T, Kim J P, Kim K, Ko H, Hwang C H and Koo K I 2019 Twelve-day medium pumping into tubular cell-laden scaffold using a lab-made PDMS connector *Eur. Cell Mater.* **38** 1–13
[25] Zhu W *et al* 2017 Direct 3D bioprinting of prevascularized tissue constructs with complex microarchitecture *Biomaterials* **124** 106–15
[26] Andrique L, Recher G, Alessandri K, Pujol N, Feyeux M, Bon P, Cognet L, Nassoy P and Bikfalvi A 2019 A model of guided cell self-organization for rapid and spontaneous formation of functional vessels *Sci. Adv.* **5** eaau6562
[27] Duong V T, Dang T T, Hwang C H, Back S H and Koo K-I 2020 Coaxial printing of double-layered and free-standing blood vessel analogues without ultraviolet illumination for high-volume vascularised tissue *Biofabrication* **12** 045033
[28] Tröndle K, Koch F, Finkenzeller G, Stark G B, Zengerle R, Koltay P and Zimmermann S 2019 Bioprinting of high cell-density constructs leads to controlled lumen formation with self-assembly of endothelial cells *J. Tissue Eng. Regen. Med.* **13** 1883–95
[29] Shi J, Mao X, Ahmed D, Colletti A and Huang T J 2008 Focusing microparticles in a microfluidic channel with standing surface acoustic waves (SSAW) *Lab Chip* **8** 221–3
[30] Shi J, Ahmed D, Mao X, Lin S-C-S, Lawit A and Huang T J 2009 Acoustic tweezers: patterning cells and microparticles using standing surface acoustic waves (SSAW) *Lab Chip* **9** 2890–5
[31] Comeau E S, Hocking D C and Dalecki D 2017 Ultrasound patterning technologies for studying vascular morphogenesis in 3D *J. Cell. Sci.* **130** 232–42
[32] Garvin K A, Dalecki D and Hocking D C 2011 Vascularization of three-dimensional collagen hydrogels using ultrasound standing wave fields *Ultrasound Med. Biol.* **37** 1853–64
[33] Serpooshan V *et al* 2017 Bioacoustic-enabled patterning of human iPSC-derived cardiomyocytes into 3D cardiac tissue *Biomaterials* **131** 47–57
[34] Armstrong J P K *et al* 2018 Engineering anisotropic muscle tissue using acoustic cell patterning *Adv. Mater.* **30** 1802649
[35] Ohlsson P, Petersson K, Augustsson P and Laurell T 2018 Acoustic impedance matched buffers enable separation of bacteria from blood cells at high cell concentrations *Sci. Rep.* **8** 9156
[36] Petersson F, Åberg L, Swärd-Nilsson A-M and Laurell T 2007 Free flow acoustophoresis: microfluidic-based mode of particle and cell separation *Anal. Chem.* **79** 5117–23
[37] Urbansky A, Ohlsson P, Lenshof A, Garofalo F, Scheding S and Laurell T 2017 Rapid and effective enrichment of mononuclear cells from blood using acoustophoresis *Sci. Rep.* **7** 17161
[38] Magnusson C, Augustsson P, Lenshof A, Ceder Y, Laurell T and Lilja H 2017 Clinical-scale cell-surface-marker

independent acoustic microfluidic enrichment of tumor cells from blood *Anal. Chem.* **89** 11954–61
[39] Jakobsson O, Oh S S, Antfolk M, Eisenstein M, Laurell T and Soh H T 2015 Thousand-fold volumetric concentration of live cells with a recirculating acoustofluidic device *Anal. Chem.* **87** 8497–502
[40] Lenshof A, Ahmad-Tajudin A, Järås K, Swärd-Nilsson A M, Aberg L, Marko-Varga G, Malm J, Lilja H and Laurell T 2009 Acoustic whole blood plasmapheresis chip for prostate specific antigen microarray diagnostics *Anal. Chem.* **81** 6030–7
[41] Koo K-I, Lenshof A, Huong L T and Laurell T 2021 Acoustic cell patterning in hydrogel for three-dimensional cell network formation *Micromachines* **12** 3
[42] Jeon O, Bouhadir K H, Mansour J M and Alsberg E 2009 Photocrosslinked alginate hydrogels with tunable biodegradation rates and mechanical properties *Biomaterials* **30** 2724–34
[43] Tahir I and Floreani R 2022 Dual-crosslinked alginate-based hydrogels with tunable mechanical properties for cultured meat *Foods* **11** 2829
[44] Nwe N, Furuike T and Tamura H 2010 Selection of a biopolymer based on attachment, morphology and proliferation of fibroblast NIH/3T3 cells for the development of a biodegradable tissue regeneration template: alginate, bacterial cellulose and gelatin *Process Biochem.* **45** 457–66
[45] Abaci A and Guvendiren M 2020 Designing decellularized extracellular matrix-based bioinks for 3D bioprinting *Adv. Healthcare Mater.* **9** e2000734
[46] Spang M T and Christman K L 2018 Extracellular matrix hydrogel therapies: in vivo applications and development *Acta Biomater.* **68** 1–14
[47] Kim B S, Das S, Jang J and Cho D W 2020 Decellularized extracellular matrix-based bioinks for engineering tissue- and organ-specific microenvironments *Chem. Rev.* **120** 10608–61
[48] Huang C C 2021 Characteristics and preparation of designed alginate-based composite scaffold membranes with decellularized fibrous micro-scaffold structures from porcine skin *Polymers* **13** 3464
[49] DeCicco-Skinner K L *et al* 2014 Endothelial cell tube formation assay for the in vitro study of angiogenesis *J. Vis. Exp.* **91** e51312
[50] Petta D *et al* 2021 Sound-induced morphogenesis of multicellular systems for rapid orchestration of vascular networks *Biofabrication* **13** 015004
[51] Hasday J D, Bannerman D, Sakarya S, Cross A S, Singh I S, Howard D, Drysdale B-E and Goldblum S E 2001 Exposure to febrile temperature modifies endothelial cell response to tumor necrosis factor-α *J. Appl. Physiol.* **90** 90–98
[52] Ashton R S, Banerjee A, Punyani S, Schaffer D V and Kane R S 2007 Scaffolds based on degradable alginate hydrogels and poly(lactide-co-glycolide) microspheres for stem cell culture *Biomaterials* **28** 5518–25
[53] Andersen T, Auk-Emblem P and Dornish M 2015 3D cell culture in alginate hydrogels *Microarrays* **4** 133–61
[54] Kim H S, Lee C-G and Lee E Y 2011 Alginate lyase: structure, property, and application *Biotechnol. Bioprocess Eng.* **16** 843
[55] Martin M, Veloso A, Wu J, Katrukha E A and Akhmanova A 2018 Control of endothelial cell polarity and sprouting angiogenesis by non-centrosomal microtubules *eLife* **7** e33864
[56] Haskard D O, Boyle J J, Evans P C, Mason J C and Randi A M 2013 Cytoprotective signaling and gene expression in endothelial cells and macrophages—lessons for atherosclerosis *Microcirculation* **20** 203–16
[57] Wallez Y and Huber P 2008 Endothelial adherens and tight junctions in vascular homeostasis, inflammation and angiogenesis *Biochim. Biophys. Acta* **1778** 794–809
[58] Bazzoni G 2011 Pathobiology of junctional adhesion molecules *Antioxid. Redox Signal.* **15** 1221–34
[59] Gao G, Park J Y, Kim B S, Jang J and Cho D-W 2018 Coaxial cell printing of freestanding, perfusable, and functional in vitro vascular models for recapitulation of native vascular endothelium pathophysiology *Adv. Healthcare Mater.* **7** 1801102
[60] Grimes D R, Kannan P, Warren D R, Markelc B, Bates R, Muschel R and Partridge M 2016 Estimating oxygen distribution from vasculature in three-dimensional tumour tissue *J. R. Soc. Interface* **13** 20160070
[61] Song W *et al* 2019 Engineering transferrable microvascular meshes for subcutaneous islet transplantation *Nat. Commun.* **10** 4602
[62] Chen S, Morita A, Sukmana I, Maeda E and Ohashi T 2015 Development of fibrin gel-microgroove model for microvascularization by endothelial cells *J. Biorheol.* **29** 19–23
[63] Kim L, Toh Y-C, Voldman J and Yu H 2007 A practical guide to microfluidic perfusion culture of adherent mammalian cells *Lab Chip* **7** 681–94
[64] Sosa J M, Nielsen N D, Vignes S M, Chen T G and Shevkoplyas S S 2014 The relationship between red blood cell deformability metrics and perfusion of an artificial microvascular network *Clin. Hemorheol. Microcirc.* **57** 275–89
[65] Parasuraman S, Raveendran R and Kesavan R 2010 Blood sample collection in small laboratory animals *J. Pharmacol. Pharmacother.* **1** 87–93